1 Introduction and Objectives

Several studies have investigated the effect of mechanical stress on microbial cell morphology and productivity in bioreactors by influencing the various morphological structures. BÜCHS and ZOELS [20] and PETER *et al.* [117] have investigated power consumption and hydrodyanmical stress in less geometrically complex systems such as shaking bioreactors. Meanwhile, in systems that are more complex from a practical standpoint, other research groups have tried to replace the biological phase with the clay-floc system due to similar physical properties and investigate the mechanical stress, as MAHNKE *et al.* [86] carried out in bubble column, PILZ and HEMPEL [119] in two- and three-phase airlift loop reactors and bubble columns, HENZLER and BIEDERMANN [52] and STINTZING *et al.* [145] in stirred tank reactors. Finally, HENZLER [51], KELLY *et al.* [57], LIN *et al.* [82], and WUCHERPFENNIG *et al.* [155] have experimentally investigated the productivity and morphology as a function of mechanical stress in the stirred tank bioreactors (STBR).

The mechanical stress mainly originates from two sources in STBRs, namely stirring and aeration through which the cells are subjected to normal and shear stress types and subsequently strained. As GRIMM *et al.* [48, 49] have suggested, the mechanical stress can further influence the morphology and even the growth of the filamentous fungi. Therefore, it is crucial to determine the magnitude and the reason for these various types of stresses.

Generally, there are two distinct ways to characterize the mechanical stress, either by measurement (experimental fluid dynamics, EFD) or by numerical simulations. The measurement techniques cannot provide a fully three dimensional stress pattern and are time consuming. However, it is possible to determine the sources of stresses, as proposed by LIN *et al.* [82], or to develop semi-empirical equations, as proposed by PILZ and HEMPEL [119], and STINTZING *et al.* [145]. Furthermore, recent efforts have provided accurate data on the mechanical stress or turbulence kinetic energy in turbulent systems by neglecting the multiphase natures and simplifying the reactor geometry [29, 45].

Because of lack of generality in experimental results and time consuming efforts, it is reasonable to use the computational fluid dynamics (CFD) in order to compute the fluid dynamical parameters. The predicted velocities and other flow dependent terms are in turn set to be post-processed so that the stress tensor is determined throughout the reactor. However, the mechanical stress caused by turbulent flows is not a parameter that

can be effortlessly determined and the less complicated turbulence models like k-ε are not suitable models in this field. Additionally, more complicated models require increasing resources in terms of computational power. The coexistence of several phases in the system elevates the difficulty level in terms of numerical approaches and various phenomena dealing with phase interactions should be considered in the simulations [59, 73, 74, 77, 112].

Another distinguished property of flow simulation in bioreactors is the difference in time scales. Most cultivations and reactions dealing with a solid biological phase last several hours or even days to occur while sudden and intermittent change of flow characteristics always necessitates describing the flows within even milliseconds. For instance, the study of VETTER [150] is focused on sequential co-simulation to couple CFD and baker yeast growth which lasts up to several days by defining a module for each area and switch from one to another to reduce the time demand. Nevertheless, the transient simulations have been carried out mostly in single phase simulations [25, 30]. Hence, despite large time scale differences, more information on flow patterns in STBRs can be gained by considering the transient effects of flows.

In the present thesis, CFD simulations are carried out in a STBR to characterize and investigate the following points:

- Quantification of the velocities and the resulting flow patterns representing most bioprocesses dealing with biopellets and exhibiting Newtonian flow behavior in both steady-state and transient-flows [113, 155]. Furthermore, the two turbulence models, namely SSG and SST models, are further assessed and their results are validated with the measured flow properties.

- Investigation of mean normal stress and the volumetric power input as global parameters which determine the mechanical stress in the entire system.

- Characterization of *real* bioreactors with non-Newtonian cultivation broths in submersed cultivation of stress sensitive *Aspergillus niger*.

- Quantification of the mechanical stress and continuous and dispersed phase flows of water/air binary flow in the STBR in both steady state and transient flow regimes.

- Comparison of various impeller types from the energy uptake point of view. The gross flow pattern for steady state flow will be determined to provide more insight into this topic.

2 Fundamentals

2.1 CFD in Stirred Tank Reactors - a Review

Stirred tank (bio-)reactors (STBR) are the most frequently used equipment in the (bio)chemical engineering. CFD provides a substantially reliable database through which the process can be optimized regarding the transport phenomena as the primary result of carrying out the CFD simulations [40]. As secondary results of carrying out the CFD simulations STBRs, the process parameters such as pH, mixing- and residence- time, nutrient concentrations, dispersed size distribution, volumetric mass transport coefficient, etc. can also be listed [78, 96, 98, 157]. As the main outcome of broad diversity of the CFD applications in STBRs, one can classify the major objectives of CFD studies in single- and multi-phase systems. In the late 1990's the bioproceses also found application in CFD studies [40].

In dealing with biochemical processes, the complexity rises due to coexistence of several phases. For instance, the cultivation medium is regarded as liquid-, microorganisms as solid and oxygen, nitrogen, carbon dioxide, etc. as gas phase [39, 40]. Furthermore, from both theoretical and practical point of view, it is more important to identify which phase is continuous and which one is dispersed. This is of paramount importance in multiphase systems, since the interfacial momentum transport and the subsequently derived equations can be considerably influenced by any assumption and simplification in this regard [54, 64, 78, 110, 137].

In single phase systems, the characterization of fluid dynamics have initially been carried out experimentally and supplied a database for further simulation which can be used for validation of simulation results qualitatively and quantitatively, as well. For example, in the works of Kresta *et al.* [68] and Schäfer *et al.* [135], the turbulence length scale has been examined in detail. This has been carried out with Laser Doppler Velocimetry (LDV) and the main measured parameters were the turbulence kinetic energy and the mean velocities. Both works also discussed the dependency of turbulence length scale on measurement grid cells and mixer diameter. The study of Schäfer *et al.* [135] shows the measurement limitations, while the other describes the fluid dynamical dependency of turbulence length scale. In the study of Mavros and Baudou [89], the important agita-

tion index was determined and the effect of impeller discharging flow is also considered. However, the definition of agitation index contributes to more practical dimensionless numbers such as power number was not discussed. This work was continued aiming to determine the fluctuation velocities and thereby the turbulence kinetic energy [90]. In addition, the switching probability of velocity vectors has been discussed, as well. Other measurement techniques such as positron emission particle tracking (PEPT) have also been evaluated in stirred tank with various types of impellers pursuing the same fluid dynamical characteristics [42]. Using experimental methods also makes the design of impellers and modification of geometries possible which in turn needs more sophisticated techniques such as three-dimensional laser Doppler anemometry to quantify the main discharge zones and the turbulence intensity by using the agitation index, hydraulic- and energetic efficiency of impellers, as investigated by Aubin *et al.* [12]. In one of the most recent studies, Galletti *et al.* [45] predicted the important Reynolds stress tensor components which is the main topic in present study, in order to provide an insight into mechanical stress in stirred tanks. They also used three-dimensional LDA and used the ensemble-averaged measurements to further examine the anisotropy and isotropy in the stirred vessel.

The validation of CFD results with experimental data makes the understanding of different turbulence dependent phenomena possible and further serves for extension of simulation data to more unknown or complex geometries. In one of the pioneer works, Ng *et al.* [105] showed how consistent the simulation with the experiments had been. The reactor was stirred with Rushton turbine and the agreement was around 60% with big deviations in turbulence kinetic energy. The authors used the sliding grid approach to connect the inner moving- and outer non-moving sections of the reactor proposed by Brucato *et al.* [18]. In a similar study, however with axial pumping impellers, Jaworski *et al.* [56] faced the same difficulties and some qualitative agreement could hardly be observed. This could be possibly due to coarse mesh used in both studies. The later attempts have been focused on stirrer type and their phenomenological fluid dynamic behavior. Khopkar *et al.* [61] tried to elucidate the difference between batch and continuous runs of stirred tank and how the continuous mode can be optimized concerning the position of impeller and that of inlet and outlet. In two separate studies by Aubin *et al.* [10, 11], other aspects of CFD simulation such as assessment of multiple reference of frames method or sliding grid, the influence of turbulence models were investigated. Moreover, Aubin *et al.* [12] carried out the grid dependency test with relatively moderate number of grid cells (from 76,000 to 350,000) and compared the results with those of previous investigations. The authors could not fully validate the results due to high inconsistency in circumferential velocities and still coarse mesh used in the study. Later

on, a more sophisticated research was undertaken by KUMARESAN and JOSHI [72] to characterize a broad range of pitched blade turbines (PBT) at various operational modes. One of the main results of this research was the assessment of more practical power- and mixing time numbers which help design the reactor more accurately. Even the normal mean stress and the scale-up criteria have been discussed.

In recent years, large eddy simulations (LES) have attracted attentions in stirred vessel simulations. This method provides a time dependent (transient) simulation and generally delivers more accurate results. ALCAMO *et al.* [2] carried out a simulation for unbaffled stirred vessel with relatively good quantitative agreement between the simulated values and the measured ones. However, the radial velocity deviated up to 75 % at certain heights in reactor coinciding with high velocity gradient regions. In order to find out, whether the LES is more beneficial than unsteady state simulation with conventional RANS, DELAFOSSE *et al.* [30] investigated the turbulence kinetic energy and the kinetic energy dissipation. They concluded that LES can capture the periodic property of turbulence kinetic energy, however the constants such as the Smagorinsky constant, plays a key role in LES approach. In another work, MURTHY and JOSHI [103] showed that despite the advantages offered by LES, one can reach almost the same results by using turbulence models from Reynolds stress model (RSM) family and save some computational resources. They further discussed the importance of two equation models such k-ε in such simulation. These models can certainly provide the preliminary results in the shortest time period.

Despite all single phase simulations gains, they cannot reflect on what exactly happens within the STBR due to existence of more complex multiphase flows which cannot be always neglected. The multiphase flows can neither be measured nor simulated as easily as single phase flows. Thus, there are more researches on this topic, although serious critics have been made considering the validity of multiphase turbulence modeling and interfacial momentum transport [110, 114]. In one of the early works, MORUD and HJERTAGER [101] carried out a two-dimensional simulation in a 15 L stirred tank reactor. They varied the gassing rate from 0.1 to 1.3 $\mathrm{m}^3_{\mathrm{gas}}\mathrm{m}^{-3}_{\mathrm{liq}}\mathrm{min}^{-1}$ (vvm) and a two phase k-ε model were used. They succeeded to qualitatively validate their results with LDA measurements. However, they did not further produce any information on the circumferential velocity, fluctuation velocities and turbulence kinetic energy. Later efforts were focused on fully three-dimensional simulations. For instance, DEEN *et al.* [28] used a single gassing rate of 0.5 vvm and a two phase particle image velocimetry (PIV) for results comparison. They further evaluated the choice of drag model, which of the Ishii-Zuber [54] or the Schiller-Naumann model [137] would result in more accurate data. This was discussed based on the form of bubbles and their distortion characteristics and the judgment went in favor of Ishii-Zuber model.

In a more theoretically challenging aspect of CFD simulations in multiphase systems, numerous efforts were devoted to characterize the interfacial momentum transfer. KHOPKAR *et al.* [62] modified the drag coefficient model of BRUCATO *et al.* [19] to obtain more accurate results. The results, however, could not predict the considerable decrease of power number observed by ZLOKARNIK [160] when the flooding takes place. In similar work, LANE *et al.* [77] had more satisfying results and more stirrer types were tested. However, the results for pitched blade turbines apparently suffered from numerical convergence problem. In another study, KHOPKAR *et al.* [60] applied their proposed drag model [62] in a more complicated geometry with triple mixer configuration. The mixing- and circulation time considerably deviated from experimental results which in turn, is due to general difficulties in flow characterization of pitched blade turbine and the unorthodox geometry of the investigated system. In binary gas/liquid simulations, one can consider the effect of internal interactions of dispersed phase particles in causing turbulence. In this regard, KHOPKAR and RANADE [63] added an additional equation to the source term leading to more satisfying outcome. Still, this approach could not easily predict the cavitation zones behind the impellers. The drag coefficient has been further modeled by including the bubble terminal rise velocity into the drag model, as carried out by SCARGIALI *et al.* [134]. They calculated the gas hold-up more accurately and the gas hold-up distribution in the reactor.

The gas/liquid simulations may not always be considered as simulations in which the dispersed phase possesses a single size distribution. Therefore, it is more convenient to take the entire size distribution into account and investigate the phenomenon how one particle from a certain size class falls in another class due to breakage or coalescence of particles. This is mostly performed by using the population balance equations (PBE) which are additional transport governing equations for internal parameters (e.g. diameter) [123]. Furthermore, how the coalescence or break up models are derived is also a cumbersome task. LANE *et al.* incorporated the model of WU [153] bubble coalescence [76]. Unfortunately, due to geometrical complexity of their system, one could not fully justify their choice of model, since there was hardly a quantitative agreement between the experiments and simulations. Thus, the first attempts were confined to easier simulations such as the effort of VENNEKER *et al.* where a two-dimensional simulation in a stirred tank of xanthane was carried out [148]. They observed that the simulation results were consistent with the measured bubble size. However, the mean velocities and their fluctuations were not discussed thoroughly.

It is clear that inclusion of the PBE's demands more computational resources due to additional differential equations. Consequently, some authors have tried to introduce approaches that fulfill the primary objectives of population balances yet require less re-

source. For instance, KERDOUSS *et al.* [59] adapted the methods of classes (CM) [71, 123] to their equations in a 2 L- reactor and validated the results for k_La and Sauter diameter. The usage of CM-method is clearly more advantageous than methods using mean normal diameter which was also observed in bubble columns by BANNARI *et al.* [13].

Other approaches such as multiple size group - (MUSIG) or bubble number density-approach (BND) serving for mathematical description of coalescence and breakage were assessed by MOILANEN *et al.* [98] and MONTANTE *et al.* [99], receptively. While the former considers the bubbles differing in size with same slip velocity, the latter solely turns the focus on the bubble density number. The BND approach produced approximately the same results as MUSIG with kinetic energy dissipation as exception. Nevertheless, both approaches are still an extra burden compared with simulations coupled with PBE without them. Therefore, in another study, KERDOUSS *et al.* [58] set the root mean squared (RMS) as convergence criterion for the residues of all transport equations equal to modest 10^{-3} due to comparatively very long time needed to reach the numerical convergence. Another approach used by GIMBUN *et al.* [47] is the quadrature method of moments (QMOM)which is the least demanding approach of the mentioned here. They applied their results for further scale-up problems and validated them with the experimental results of DEEN *et al.* [28]. However, no bubble size distributions were provided, since this approach simply assumes all bubbles of the same size are and the momentum transfer between phases is determined by this single diameter.

In case of solid particle as dispersed phase, the approaches are the same as gas/liquid-simulations. However, the solid phase cannot be considered as continuum any more. Hence, the Euler-Euler may not be as suitable Euler-Lagrange method. Moreover, the density difference is the main index separating the solid/liquid- from the gas/liquid- simulations. Still, the interfacial momentum transfer emerges as the main challenge here, too.

Early attempts were devoted to the methodological investigations in terms of exploring the suitable approach. For instance, MICALE *et al.* [96] evaluated two models; the settling velocity model (SVM) and the multi fluid model (MFM). In SVM, the solid phase builds a cluster of particle sinking and rising in the fluid and do not have any impact on the continuous phase, whereas in MFM the momentum transport equations are extended, so that the influence of the dispersed phase can be correctly showed. The authors concluded that up to a solid phase concentration of $10\,\mathrm{kg\,m^{-3}}$ both models perform at same level. However, the SVM fails to predict the solid phase profiles in concentrations beyond $10\,\mathrm{kg\,m^{-3}}$. In other studies, the drag force- and drag coefficient- models were

modeled by algebraic models. ALTWAY *et al.* [6] used an algebraic slip model (ASM) to assess the various particle size and mass fractions. The results revealed that higher accuracy can be reached if the flow is simply laminar and the periodic boundary conditions are not included in the system. This was also confirmed by SAEED *et al.* [131] where even the shape and size of caverns [85] in non-Newtonian fluids is given correctly.

In solid/liquid- simulations, the suspension height is an important parameter in process design. MICALE *et al.* [95] tried to simulate the experimental results of BUJALSKI *et al.* [21] with their proposed MFM model. The suspension height was in good agreement with the experimental results, while the simulated and measured power number significantly differed from each other. This is due to underestimation of mean velocities and their fluctuation values. The major cause of this finding was, according to LJUNGVIST *et al.* [83], the drag models do not suit to this type of simulations and the Euler-Euler approach, either. Their results were observed by OCHIENG and ONYANGO [106] later. However, they showed that the realistic solid mass fraction is still the modest 1 % in cases where the flow is fully turbulent.

The most desirable objective in simulations is to take all phases into account. As mentioned earlier, most (bio-)chemical processes are dealing with three or sometimes more phases [39]. However, there are serious doubts in credibility of models implemented in such simulations. For instance, MURTHY *et al.* [102] tried to evaluate the criterion proposed by BOHNET and NIESMAK [15]. Despite successful implementation of the criterion, the authors did not provide any further information on experimental validation of flow patterns. The critical impeller speed as a function of particle diameter to fully disperse the particles was investigated by MURTHY *et al.* and PANNEERSELVAM *et al.* [104, 112]. They used experimental data of binary measurements and made remarks on mass transport within the system.

In case of more sensitive biological systems, one faces severe challenges on both simulation and measurement (validation) levels. This is due to several parameters and phenomena such as cell- growth and -lysis, viscosity and rheological changes of cultivation media, turbidity of media, etc. However, the efforts of GHADGE *et al.* [46] and LAPIN *et al.* [78] were concentrated on biotechnological processes. While the former investigated the production of cellulase and determined the specific power input and global normal stresses, the latter simulated the glucose uptake by *Escherchia coli* in a STBR. They used a reduced biological network proposed by CHASSAGNOLE *et al.* [23] and used Euler-Lagrange approach. Their effort resulted in a time dependent substrate uptake scheme in the system, whereas any fluid dynamical prediction was not tested against the reality. In later works, XIA *et al.* [157] carried out the simulation with various process parameters such as

impeller type, in order to optimize the productivity of avermectin by *Streptomyces avermitilis*. They simultaneously determine the morphology as supporting parameter to have a better understanding of the system. Despite missing information on fluid dynamical validation, the above mentioned studies shows the path towards simulation of biological systems and the confronting challenges.

2.2 Governing Equations

This section will discuss fundamental equations and discretization schemes, the numerical approaches in single phase and multiphase flows, and the existing models in rheological studies. The governing equations to be solved in CFD are the differential or integral forms of mass, momentum- and energy conservation laws. It is noteworthy to mention that the conservation equations are primarily used for an infinitesimal amount of mass, known as control mass. However, since it is rather impractical to follow a rapidly passing parcel of fluid within boundaries of interest, a certain region with a known volume will be defined and the balance equations are written for fluxes entering and exiting through the surfaces of this region. As a result of this approach, the control mass is replaced by a control volume [43, 44]. In addition, in the control volume approach, the properties are intensive, which means that the balance equations are independent from the amount of the matter. Generally, an intensive property φ for the conservation parameter Φ is defined as the following

$$\varphi \equiv \frac{\Phi}{m} \tag{2.1}$$

with m denoting the mass. It is obvious that in this approach, $\varphi = 1$ and $\varphi = \mathbf{u}$ for mass and momentum, respectively, while $\mathbf{u}$ is the velocity vector. Using this approach allows deriving the so called Reynolds transport theorem or control volume equation. This equation restates the accumulation term within the control mass in a valid form for control volume and its surrounding boundaries, the so called control surfaces, shown in **Figure 2.1**.

$$\frac{\mathrm{d}}{\mathrm{d}\,t}\int\limits_{V_{CM}} \rho\,\varphi\,\mathrm{d}V = \frac{\mathrm{d}}{\mathrm{d}\,t}\int\limits_{V_{CV}} \rho\,\varphi\,\mathrm{d}V + \int\limits_{S_{CV}} \rho\,\varphi\,(\mathbf{u}-\mathbf{u}_b)\cdot\mathbf{n}\,\mathrm{d}S \tag{2.2}$$

where V_{CM} is the volume of control mass, V_{CV} and S_{CV} denote the volume and surface of the control volume, respectively. The relative motion between fluid parcels and the control volume is assigned by the term in parenthesis in second integral on the right hand side of the equation. This equation implies that the rate of change of an intensive property in the control mass is equal to its rate of change in the control volume plus the net

flow through the boundaries due to relative motion. The latter is known as convective (advective) term, as well [14, 124].

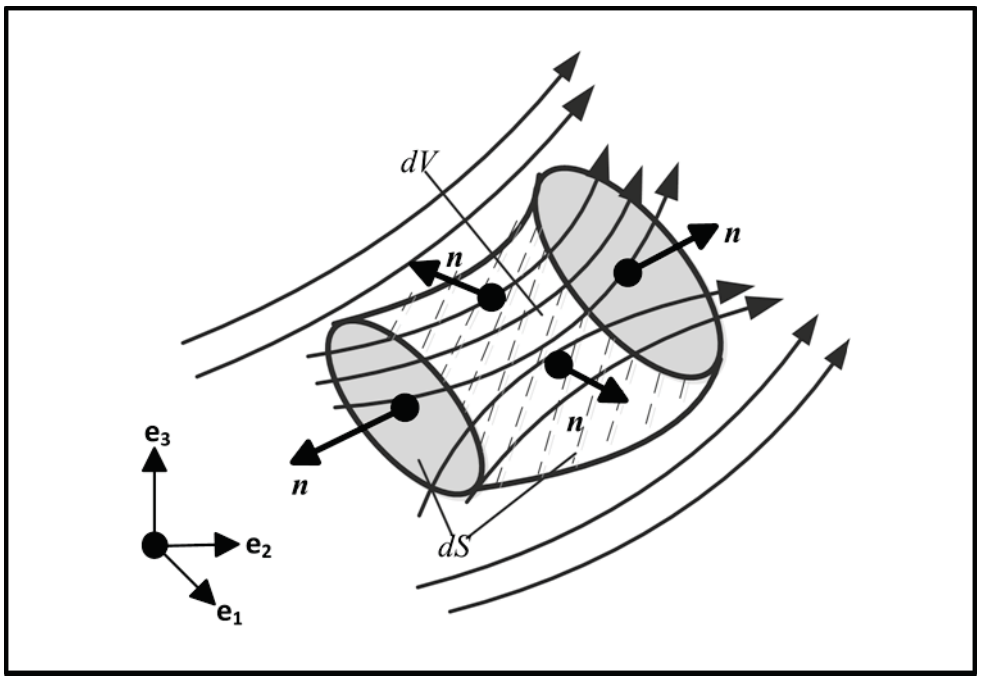

Figure 2.1: Streamlines, control volume and control surfaces in an infinitesimal balance element in control volume approach

The mass conservation, also known as the continuity equation, is pivotal in all CFD problems and will be discussed in the following. Indeed, the intensive mass value is equal to unity. Furthermore, the mass balance is without the generation term (sink or source terms), as it is not in the scope of the present work at any stage

$$\frac{\partial \rho}{\partial t} + \nabla \cdot (\rho \, \mathbf{u}) = \frac{D\rho}{Dt} = 0 \tag{2.3}$$

The left hand side of the equation (2.3) is better known as the substantial derivative, which takes both the local change of the parameter (in this case density) and its rate into account. In other words, the motion of fluid parcels, in this case the control volume, serves for the local change of the density gradient in the system.

The momentum conservation equation, also known as the equation of motion, looks relatively more complicated than the continuity equation. Generally, the momentum conservation equations are derived in a way similar to the way the continuity equations are written. However, the convective terms and the viscous terms appear in more complicated tensor forms. The fully expanded momentum conservation equation can be written as the following for Cartesian coordinates:

$$\rho \frac{Du_x}{Dt} = -\frac{\partial}{\partial x}\Big[2\mu \frac{\partial u_x}{\partial x} - \frac{2}{3}\mu(\nabla \cdot \mathbf{u})\Big] + \frac{\partial}{\partial y}\Big[\mu\big(\frac{\partial u_x}{\partial y} + \frac{\partial u_y}{\partial x}\big)\Big] + \frac{\partial}{\partial z}\Big[\mu\big(\frac{\partial u_x}{\partial z} + \frac{\partial u_z}{\partial x}\big)\Big] + \rho\, g_x - \frac{\partial p}{\partial x} \tag{2.4a}$$

$$\rho \frac{Du_y}{Dt} = -\frac{\partial}{\partial y}\Big[2\mu \frac{\partial u_y}{\partial y} - \frac{2}{3}\mu(\nabla \cdot \mathbf{u})\Big] + \frac{\partial}{\partial x}\Big[\mu\big(\frac{\partial u_y}{\partial x} + \frac{\partial u_x}{\partial y}\big)\Big] + \frac{\partial}{\partial z}\Big[\mu\big(\frac{\partial u_y}{\partial z} + \frac{\partial u_z}{\partial y}\big)\Big] + \rho\, g_y - \frac{\partial p}{\partial y} \tag{2.4b}$$

$$\rho \frac{Du_z}{Dt} = -\frac{\partial}{\partial z}\Big[2\mu \frac{\partial u_z}{\partial z} - \frac{2}{3}\mu(\nabla \cdot \mathbf{u})\Big] + \frac{\partial}{\partial x}\Big[\mu\big(\frac{\partial u_z}{\partial x} + \frac{\partial u_x}{\partial z}\big)\Big] + \frac{\partial}{\partial y}\Big[\mu\big(\frac{\partial u_z}{\partial y} + \frac{\partial u_y}{\partial z}\big)\Big] + \rho\, g_z - \frac{\partial p}{\partial z} \tag{2.4c}$$

For the sake of simplicity, the equations 2.4 are written in vector form:

$$\rho \frac{D\mathbf{u}}{Dt} = -\nabla \cdot \boldsymbol{\tau} - \nabla p + \rho\, \mathbf{g} \tag{2.5}$$

As mentioned earlier, the left hand side of equation denotes the rate of momentum change due to the convective flow and the local momentum rate per unit volume. The dynamic viscosity emerges as μ in this equation. The first terms on the right hand side are the viscous forces per unit volume and the last two terms are forces exerted due to the pressure gradient and gravitational forces respectively.

It is assumed that the stress tensor is symmetrical, implying that $\tau_{ij} = \tau_{ji}$ [124], and this assumption does not violate the modeling approaches in the following chapters. The components of the stress tensor are defined as the following

$$\tau_{xx} = 2\mu \frac{\partial u_x}{\partial x} - \frac{2}{3}\mu \nabla \cdot \mathbf{u} \tag{2.6a}$$

$$\tau_{yy} = 2\mu \frac{\partial u_y}{\partial y} - \frac{2}{3}\mu \nabla \cdot \mathbf{u} \tag{2.6b}$$

$$\tau_{zz} = 2\mu \frac{\partial u_z}{\partial z} - \frac{2}{3}\mu \nabla \cdot \mathbf{u} \tag{2.6c}$$

$$\tau_{xy} = \tau_{yx} = \mu\big(\frac{\partial u_y}{\partial x} + \frac{\partial u_x}{\partial y}\big) \tag{2.6d}$$

$$\tau_{xz} = \tau_{zx} = \mu\big(\frac{\partial u_z}{\partial x} + \frac{\partial u_x}{\partial z}\big) \tag{2.6e}$$

$$\tau_{yz} = \tau_{zy} = \mu\big(\frac{\partial u_y}{\partial z} + \frac{\partial u_z}{\partial y}\big) \tag{2.6f}$$

In CFD, there are two special cases of the motion equation which are frequently used as listed below:

(i) The Navier-Stokes equation: The equation of motion will be simplified, if the fluid density and viscosity are constant. This equation is the fundamental equation in the present work. The difficulties arise in solving the Navier-Stokes equation necessitates using appropriate and feasible modeling at different steps of solution

$$\rho \frac{D\mathbf{u}}{Dt} = -\mu \nabla^2 \mathbf{u} - \nabla p + \rho \mathbf{g} \tag{2.7}$$

The main property of this equation is its non-linearity in the most general form due to the gradients of the stress tensor and bulk flow momentum

(ii) The Euler equation: if the viscous forces are negligible or very small compared with the convective forces.

$$\rho \frac{D\mathbf{u}}{Dt} = -\nabla p + \rho \mathbf{g} \tag{2.8}$$

In turbulence flows, due to the unsteady and intermittent nature of macro- and micro-eddies and complex boundary conditions, there is no analytic solution for either Navier-Stokes or Euler equations. Therefore, numerical methods are applied and then will be commenced with discretization of the differential equations and meshing the simulation geometries.

2.2.1 Numerical Grid and Discretization

The first and most important step in the numerical solution of governing equations is to split the solution domain in subdomains according to prescribed dimensions that may not exceed the physical boundaries of the original geometry of interest. There are various types of such grids that will be chosen based on geometrical complexity and simulation demands.

(i) *Structured grid*: if the grid lines of one family do not cross their counterparts from other families, or cross them just once, a structured grid will be obtained. So, the grid nodes will be notated as the Cartesian coordinate system and each node would have just 2, 4 and 6 neighbor nodes in a 1-, 2- and 3-D grid, respectively (cf. **Figure 2.2**). There is not much numerical difficulty in terms of the consistency of algorithms with this type of grid and the numerical matrix of algebraic equation has a regular structure, which is suitable for most algorithms consuming usually less computational resources. However, one cannot easily control the distribution of grid nodes due to a 1:1 correspondence between the grid lines of each family and

this would lead to either an over-dense mesh or an inflation of grid nodes in regions where the mesh density does not need to be quite high.

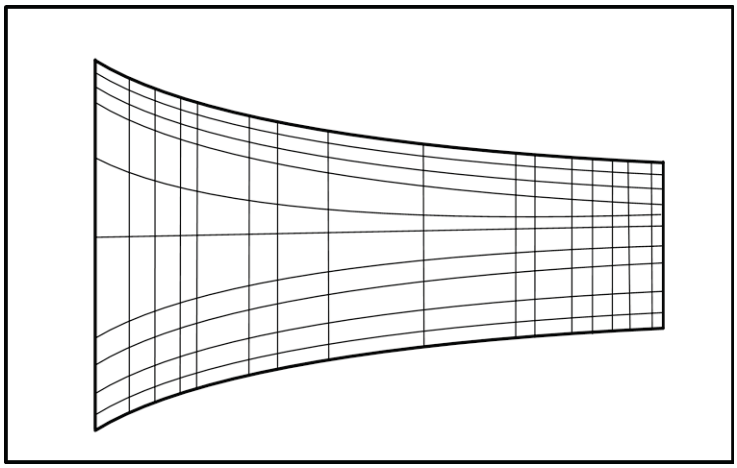

Figure 2.2: A two-dimensional structured grid for a nozzle

(ii) *Block-structured grid*: unlike structured grids, the block-structured grids are distinguished through internal, or sometimes external, blocks that shape the entities in the solution domain. These blocks will be further meshed and may or may not overlap each other. An example is **Figure 2.3**, where the inner part is an ellipsoidal block lying in the nozzle. Each block can be treated individually with its own grid size. As a result of this conception, it is easier to control the nodal distribution throughout the grid. Furthermore, the grid nodes of each block may match or mismatch at interfaces. The mismatched interfaces would offer more flexibility in meshing, whereas the numerical solution can be compromised.

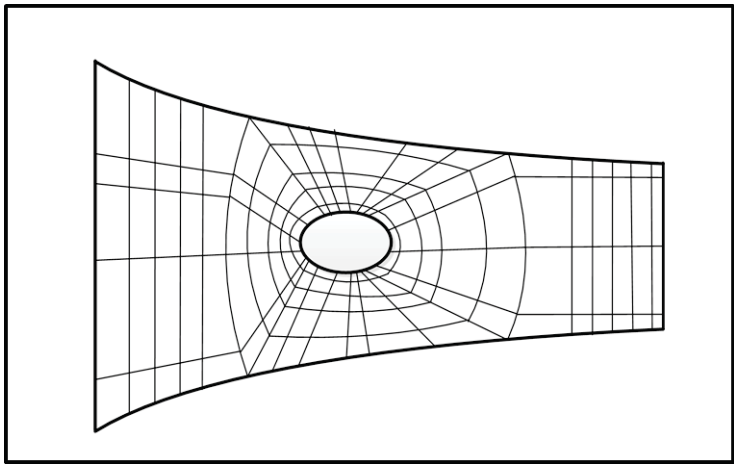

Figure 2.3: A two-dimensional block-structured grid with matching interfaces

(iii) *Unstructured grid*: this type of grid realizes maximum flexibility with respect to controlling the distribution of grid refinement. The grid cells do not necessarily possess any prescribed shape, as depicted in **Figure 2.4.** Still, dealing with the resulting matrices of discretized equations is not effortless and many modifications should be implemented. The more complex geometries suit the unstructured grids the most, although one can save time and use an unstructured mesh for relatively less complicated geometries in order to obtain preliminary results for detailed case studies.

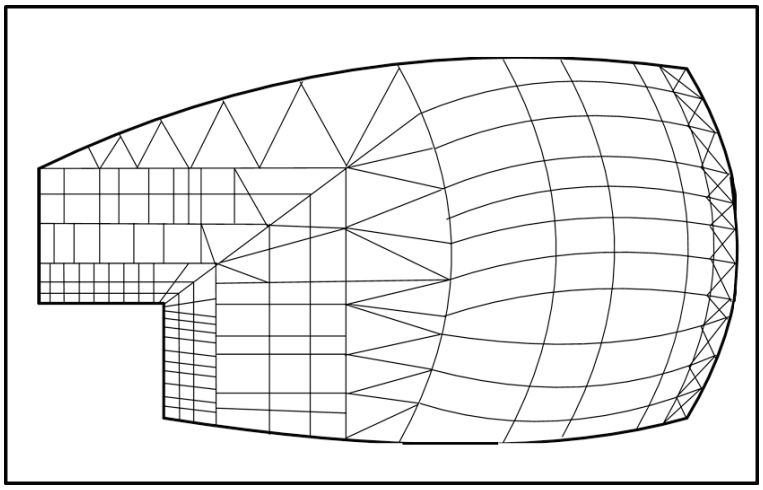

Figure 2.4: A two-dimensional unstructured grid with arbitrary grid cell size

In dealing with the numerical solution of governing equations in transport phenomena, one can choose between three different methods; these methods serve for the discretization of governing equations and converting the differential equations into algebraic equation systems. The three distinctive methods used in this purpose are the finite difference (FD), the finite volume (FV), and the finite element (FE) method. In CFD, and particularly in incompressible flows, the FV method is the most frequently used method delivering reliable results.

In FV method, as its name suggests, one determines the transport characterizing parameters in control volumes. The conservation equations are set to be solved for each control volume in the solution domain are in integral form

$$\underbrace{\int_S \rho\,\varphi\,\mathbf{u}\cdot\mathbf{n}\,\mathrm{d}S}_{\text{convective flux}} = \underbrace{\int_S \Gamma\,\nabla\varphi\cdot\mathbf{n}\,\mathrm{d}S}_{\text{diffusive flux}} + \underbrace{\int_V q_\varphi \mathrm{d}V}_{\text{source/sink}} \tag{2.9}$$

Under this approach, the surface integrals of diffusive and convective terms in equation 2.9 must be obtained for all faces of the control volume. Hence, the surface integral is

the sum of integrals at all faces. Let's simplify the integrand of convective and diffusive fluxes as f^c and f^d, respectively. The surface integral can be approximated as following

$$\int_S f \,\mathrm{d}S = \sum_i \int_{S_i} f \,\mathrm{d}S \tag{2.10}$$

As depicted in **Figure 2.5**, the integral at each face (n, s, e, w) can be solved, if the respective integrand at each face is known. However, the integrand is just known at nodes (P, N, S, E, W) and can be approximated at intersections. Hence, the integral at the exemplary face w is estimated by using the Simpson's rule which is a fourth-order approximation:

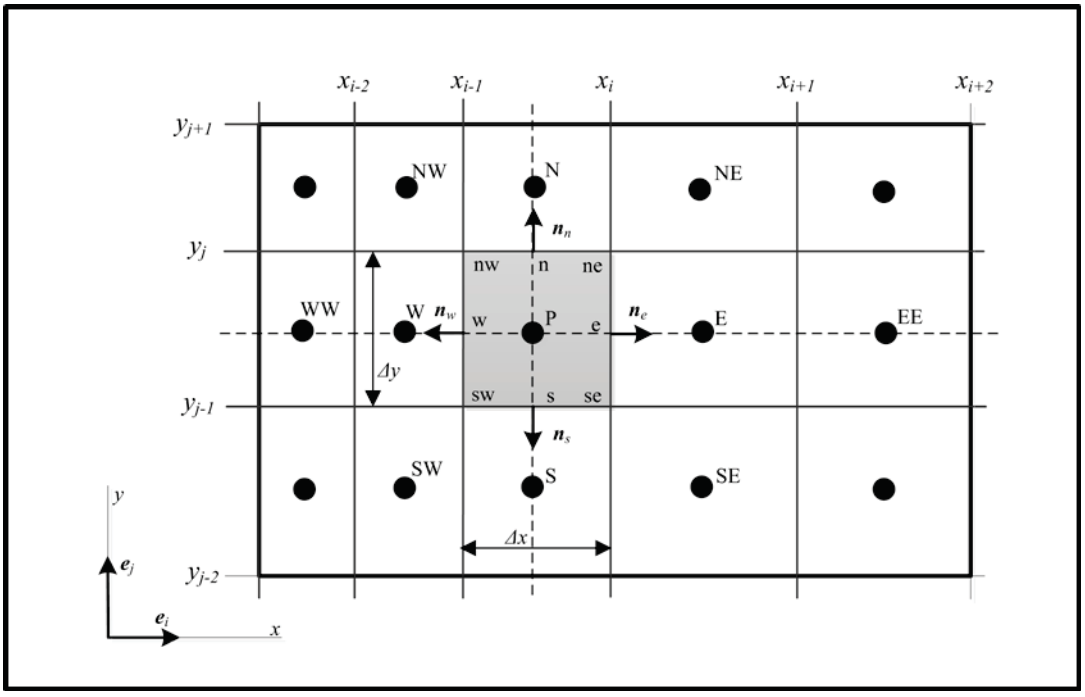

Figure 2.5: Typical 2D control volume with nodal and facial notations for numerical grid

$$\int_{S_w} f \,\mathrm{d}S \approx \frac{S_e}{6}\left(f_{nw} + 4f_w + f_{sw}\right) \tag{2.11}$$

The volume integral for the sink or source term is relatively more demanding, since the only known value for this term is at the centroid P and a fourth order approximation can also be used to estimate the total volume integral for an uniform Cartesian grid:

$$Q_P = \int_V q \,\mathrm{d}V \approx \frac{\Delta x\,\Delta y}{36}\left(16q_P + 4q_s + 4q_n + 4q_w + 4q_e + q_{se} + q_{sw} + q_{ne} + q_{nw}\right) \tag{2.12}$$

There are several other methods to approximate the integral for transport terms at each face as there are source or sink terms for each control volume [43, 114, 149]. Nevertheless, the integrand values at nodes w , nw, sw, and se and faces n, s, e, and w are not known. Therefore, interpolations should be carried out so that the approximations (equations 2.11 and 2.12 can be concluded. Of the various schemes applied in this field, this work uses the more complex one. For instance, the Quadratic Upwind Interpolation for Convective Kinematics (QUICK) uses a parabolic [80] dependency between nodal values to estimate the values at each face.

$$\varphi_e = \begin{cases} \varphi_P + g_1\left(\varphi_E - \varphi_P\right) + g_2\left(\varphi_P - \varphi_W\right) & \text{for } u_x > 0 \\ \varphi_E + g_3\left(\varphi_P - \varphi_E\right) + g_4\left(\varphi_E - \varphi_{EE}\right) & \text{for } u_x < 0 \end{cases} \tag{2.13}$$

where the coefficients g_1, g_2, g_3 and g_4 can be obtained as following

$$\begin{aligned} g_1 &= \frac{(x_e - x_P)(x_e - x_W)}{(x_E - x_P)(x_E - x_W)} \;; & g_2 &= \frac{(x_e - x_P)(x_E - x_e)}{(x_P - x_W)(x_E - x_W)} \\ g_3 &= \frac{(x_e - x_E)(x_e - x_{EE})}{(x_P - x_E)(x_P - x_{EE})} \;; & g_4 &= \frac{(x_e - x_E)(x_P - x_e)}{(x_E - x_{EE})(x_P - x_{EE})} \end{aligned} \tag{2.14}$$

Or higher-order schemes are also useful, particularly if the integrals are also approximated by using higher-order formulae. For instance, suppose that the functionality of φ is described by polynomial degree three

$$\varphi(x) = a_0 + a_1 x + a_2 x^2 + a_3 x^3 \tag{2.15}$$

One can apply four neighboring nodes of face e, namely W, P, E and EE, in order to determine the a_i coefficients. In a totally uniform Cartesian grid, the value φ_e reads

$$\varphi_e = \frac{27\varphi_P + 27\varphi_E - 3\varphi_W - 3\varphi_{EE}}{48} \tag{2.16}$$

The derivatives for diffusive term are calculated by the first differentiation of polynomial fit function:

$$\left(\frac{\partial \varphi}{\partial x}\right)_e = a_1 + 2a_2 x + 3a_3 x^2 \tag{2.17}$$

and by using the same approach as above the approximated derivative is

$$\left(\frac{\partial \varphi}{\partial x}\right)_e = \frac{27\varphi_E - 27\varphi_P + \varphi_W - \varphi_{EE}}{48\Delta x} \tag{2.18}$$

However, since in Navier-Stokes equations the velocity field is unknown, one faces a further problem in approximating and interpolating the terms. This is also known as the velocity-pressure coupling problem [114, 122, 149]. Generally speaking, particularly in

incompressible flows, there is no relationship between the pressure field and the velocity with fluid density. This implies that the pressure determined either by the continuity or equation of motion must fit in the other one.

One of the many possibilities to avoid physically invalid predictions in terms of either the pressure or velocity field is to use a staggered grid. This type of grid is essential for unstructured or block-structured grids [115]. Therefore, while one of the equations is adapted to the cells of the staggered grid, the other set of equations is solved in the primary grid. According to PASCHEDAG [114] and PATANKAR [115], the algorithm is iterative and results in physically reasonable results. However, it can suffer from the oscillating pressure field.

2.2.2 Boundary Conditions

Boundary conditions are crucial in closing the discretized equation system. Otherwise one cannot reach a solution to this problem. Physically, the boundary conditions represent the influence of the environment on the solution domain. If transient simulation is carried out, additional initial conditions are also needed. Mathematically, there are three sorts of boundary conditions that help in determining integration constants [14, 43, 114, 144, 151].

(i) *Dirichlet boundary condition*: this is the most common and easiest boundary condition and assumes that the parameter φ is known at certain points, faces, etc.

$$\varphi|_{BC} = C_1 \tag{2.19}$$

(ii) *Neumann boundary condition*: if the gradient of parameter is known, then this type of condition is applied. Some common examples of Neumann conditions include the conducted heat at the walls of an isolation jacket and the shear stress estimated at walls.

$$\frac{\partial \varphi}{\partial x}|_{BC} = C_2 \tag{2.20}$$

where x refers to the Cartesian coordinate in the same direction of the normal vector to boundary.

(iii) *Cauchy boundary conditions*: in this work, no boundary conditions satisfy the Cauchy boundary condition. However, it is quite possible that in heat transfer the temperature and the temperature gradient can be estimated via the following equation:

$$\frac{\partial \varphi}{\partial x}|_{BC} + C_3 \varphi|_{BC} = C_4 \tag{2.21}$$